Eng. Sci., 2025, **35**, 1593

Engineered Science
DOI: https://dx.doi.org/10.30919/es1593

Omni-Surface Hydrophobic Bamboo Composite with Enhanced Antibacterial and Self-Cleaning Performance

Zixuan Wang,[1, 2,#] Yanfang Tan,[1, 2,#] Chun Shi,[1,*] Hanhui Lei,[3] Terence X. Liu,[3] Mohamed Kallel[4,*] and Zhengjun Shi[1, 2,*]

Abstract

The nutrients within bamboo are prone to absorbing moisture, which creates an environment conducive to mold growth and restricts the expanded use of bamboo. Although traditional hydrophobic coatings can impart superhydrophobic properties to the surface of bamboo, they are unable to penetrate its interior structure, thereby leaving the intrinsic hydrophilicity of bamboo unaltered. In this study, we have engineered an omni-surface hydrophobic bamboo exhibiting anti-mold and super-hydrophobic properties through a methodology encompassing liquid deposition, hot pressing, and surface spraying techniques. The findings reveal that the water contact angle on the outer surface is 161.16°, the inner surface measures 135.47°, and the sliding angle of the outer surface is a mere 8°. Notably, the bamboo was endowed with exceptional anti-mold qualities by the omni-surface hydrophobic treatment, which greater than 99% control efficacy against *Aspergillus niger*, *Trichoderma viride*, and *Penicillium citrinum.* An omni-surface hydrophobic bamboo composite (SHDB-Ag-S) exhibiting superior pat of natural bamboo and its Young's modulus is 1.37 times that of natural bamboo. The omni-surface hydrophobic bamboo developed in this study demonstrates considerable potential for applications in architecture and interior design due to its mold-resistant and self-cleaning properties.

Keywords: Mildew resistant; Omni-surface hydrophobic; Liquid phase deposition; Self-cleaning performance.
Received: 22 April 2025; Revised: 26 May 2025; Accepted: 28 May 2025.
Article type: Research article.

1. Introduction

The escalating issue of plastic pollution necessitates the urgent identification of renewable resources to replace plastics.[1] In the context of facilitating transition in its energy structure, achieving peak carbon emissions, and attaining carbon neutrality, the development of renewable materials as alternatives to plastics is critically important.[2] Such materials not only reduce reliance on fossil fuels but also steer energy consumption towards a more sustainable and low-carbon future.[3] Bamboo emerges as a particularly promising renewable resource due to its exceptional strength, rapid growth cycle, and high yield.[4] By enhancing the hydrophobic properties of bamboo, it is possible to effectively prevent water and microbial intrusion, thereby minimizing the risk of mold growth, extending the lifespan of bamboo products, and broadening their potential applications.[5]

Superhydrophobicity is a unique surface property that allows the surface to successfully reject liquids, including water, due to its extraordinarily low affinity for water.[6] This property is typically quantified by a water contact angle exceeding 150°, with a sliding angle generally below 10°.[7] Consequently, water droplets can easily roll off superhydrophobic surfaces, carrying away dust and other particles, thereby minimizing the adherence of microorganisms such as mold.[8] Various methodologies have been developed to fabricate superhydrophobic surfaces, including chemical vapor deposition (CVD), the sol-gel method, lamination assembly technology, plasma treatment, and the direct creation of micro/nano-scale rough structures on material surfaces through micro/nano-fabrication techniques.[9] Although there are many research methods discussed earlier,

[1] *Yunnan Provincial Key Laboratory of Wood Adhesives and Glued Products, Southwest Forestry University, Kunming 650224, China*
[2] *Key Laboratory of State Forestry and Grassland Administration on Highly-Efficient Utilization of Forestry Biomass Resources in Southwest China, Southwest Forestry University, Kunming 650224, China*
[3] *Department of Mechanical and Construction Engineering, Northumbria University, Newcastle Upon Tyne, NE1 8ST, UK*
[4] *Department of Physics, College of Science, Northern Border University, Arar, 73222, Saudi Arabia*
[#] *These authors contributed to this work equally.*
[*] *E-mail:* shizhengjun1979@swfu.edu.cn (Z. Shi);
shichun@swfu.edu.cn (C. Shi);
Mohamed.Kallel@nbu.edu.sa (M. Kallel)

there are still some deficiencies. CVD is usually carried out at high temperatures, which may cause damage to heat-sensitive substrate materials and limit its application in certain industries.[10] The sol-gel method faces many challenges in scale-up production, such as high equipment requirements and great difficulty in process control. Due to its sensitivity to reaction conditions, it is difficult to ensure the uniformity and consistency of the products during large-scale production.[11] The impregnation method involves immersing the base material in a solution containing superhydrophobic modifiers, and then completing the modification through simple processing steps such as drying.[12] It does not require complex equipment or advanced technology, is easy to implement, and is very convenient for both large-scale production and laboratory research.[13] Therefore, this experiment is more suitable for the immersion method. In a study by Lu et al., micro/nanocomposite structures were synthesized on bamboo surfaces using metal-organic framework (MOF) materials as a template via in situ growth and conversion processes.[14] This approach facilitated the application of sodium laurate to the bamboo surface, thereby reducing surface energy and establishing a superhydrophobic layer. Although bamboo gained superhydrophobicity and other desired qualities from the surface treatment, the hydrophobic coating only covers the outside of the bamboo, leaving its interior naturally hydrophilic.[15] This limitation of hydrophobic properties to the surface constrains bamboo's utility in applications requiring thorough hydrophobicity. Mael Nicolas synthesized a perfluoroalkyl alkyl pyrrole monomer that, upon electro polymerization, produces a surface with a multi-scale rough structure, demonstrating stable superhydrophobicity in both pure water and under acidic and basic conditions.[16] Conversely, perfluoroalkyl methane sulfonates exhibit prolonged environmental persistence due to their high stability and resistance to biodegradation.[17] These compounds pose significant risks to human and wildlife health due to their potential for bioaccumulation through the food chain.[18] Furthermore, many superhydrophobic coatings may become unstable or degrade when exposed to acids, bases, or other chemicals, as well as under mechanical stress and abrasion.[19] The insufficient durability of superhydrophobic surfaces or coatings severely limited their use in harsh environments or industrial settings.[20] The insufficient durability of superhydrophobic surfaces or coatings severely limited their use in harsh environments or industrial settings.[21] A multifaceted approach that includes research and innovation in materials science, surface science, chemical engineering, and environmental science is required to address these issues and challenges.[22]

The hydrophobic properties of bamboo can be significantly enhanced through an omni-surface hydrophobic modification of its entire surface. This modification reduces water retention on the bamboo surface, thereby hindering mold adhesion and subsequently decreasing the likelihood of mold proliferation.[5] The water absorption of bamboo can be reduced by omni-surface hydrophobic modification, which is key to maintaining its size and shape stability.[23] The acyl chloride group (-COCl) is a reactive chemical group that can interact with a variety of hydrogen-containing compounds, including alcohols and amines. Consequently, it is suitable for chemically modifying a broad spectrum of materials.[24] Because of its low surface energy characteristics, stearoyl chloride is a popular chemical molecule that is frequently employed to give materials hydrophobicity. Furthermore, stearoyl chloride exhibits long-lasting efficacy as a modifier, attributed to its chemical stability at room temperature and its resistance to reacting with environmental compounds.[25] Because of these qualities, stearoyl chloride is frequently utilized in the rubber, plastics, coatings, adhesives, textile, and paper industries, particularly to increase the materials' hydrophobicity, wear resistance, and protection. Chlorine atoms from stearoyl chloride can coprecipitate with $AgNO_3$ to create AgCl nanoparticles (AgCl NPs). The surface of the bamboo has become extremely rough and hydrophobic by the deposition of AgCl NPs.[26] Silver chloride nanoparticles (AgCl NPs) exhibit the ability to bind to bacterial plasma membranes, enhance bacterial cells' adaptability to membrane perforation, and induce the generation of free radicals and reactive oxygen species (ROS), thereby inhibiting the proliferation of bacteria and mold.[27] Despite their broad-spectrum antibacterial properties, AgCl NPs are infrequently employed for mold control and the treatment of hydrophobic bamboo.

Superhydrophobicity can be achieved by increasing surface roughness and reducing surface energy. The AgCl NPs formed by the chlorine atoms provided by stearyl chloride and the Ag(I) provided by $AgNO_3$ create certain protrusions and textures on the surface of bamboo materials, thereby increasing the surface roughness. This rough surface structure is conducive to increasing the contact angle with water, making it more difficult for water to spread on the bamboo surface and enhancing the hydrophobicity of the bamboo from a geometric perspective. Stearyl chloride molecules contain long-chain alkyl groups. After being grafted onto the surface of bamboo through chemical reactions, the long-chain alkyl groups will form a low-energy surface layer on the surface of the bamboo. Due to the non-polar nature of long-chain alkyl groups, the affinity of the bamboo surface for polar water molecules is reduced, thereby effectively lowering the surface energy of the bamboo.[28] Low surface energy materials usually exhibit superhydrophobic properties. The rough surface structure combined with the low surface energy organic layer can further increase the contact angle between the bamboo surface and water, thereby significantly enhancing the hydrophobicity of the bamboo.[29] AgCl NPs deposited on the surface of bamboo have good bactericidal and antibacterial properties. This characteristic enables the bamboo that has been synergistically modified not only to have excellent hydrophobicity but also to reduce the possibility of bacterial growth and mold, extend the service life of the bamboo, and

broaden the application fields of bamboo.

Consequently, there is a critical need to develop bamboo materials with improved durability, dimensional stability, and hydrophobic characteristics across omni-surfaces. This study aims to create such bamboo materials by modifying their surface properties, specifically by increasing surface roughness and reducing surface energy to achieve omni-surface hydrophobicity. We have rigorously investigated the impact of this omni-surface hydrophobic bamboo on mold control, as well as several key operational factors that may influence the longevity of the superhydrophobic layer. An innovative method for the creation, processing, and use of bamboo protection is provided by the omni-surface hydrophobic alteration, which effectively improves the antifungal qualities of bamboo (Fig. 1).

2. Materials and methods

2.1 Experimental material

The main rods of Dendrocalamus giganteus, which were three years old and free from mildew and insects, were collected in Lincang City, Yunnan Province. Following the removal of the bamboo's outer green and inner yellow layers, the material was processed into pieces measuring 50 × 20 × 2 mm³ and subsequently dried at 103 ± 2°C until a constant weight was achieved. The reagents used in the experiment, such as sodium hydroxide (NaOH, ≥ 96%), anhydrous sodium sulfite (Na_2SO_3), silver nitrate ($AgNO_3$), stearoyl chloride, toluene, ethanol (≥ 99.7%), sucrose, and agar, were all purchased from Macklin Biochemical Technology Co., Ltd. (Shanghai, China) and Sinopharm Chemical Reagent Co., Ltd. (Shanghai, China). All reagents and solvents are AR grade and can be used without further separation or purification. The experimental strains of *Aspergillus niger, Trichoderma viride, and Penicillium citrinum* (*A. niger, T. viride, and P. citrinum*) were provided by the Microbiology Laboratory of Southwest Forestry University. The distilled water used in the experiment was made by the laboratory.

2.2 Pretreatment of bamboo

The natural bamboo (NB) samples underwent an initial treatment involving immersion in a solution of NaOH (2.5 M) and Na_2SO_3 (0.4 M) at 70 °C for a duration of 2 hours. This was followed by extensive rinsing with deionized water until a neutral pH was attained. The treated samples were then subjected to freeze-drying and labeled as pre-DB.

2.3 Modification

Subsequently, pre-DB samples were immersed in a 0.1 M $AgNO_3$ solution and subjected to a vacuum of –0.075 MPa for 2 hours to ensure the solution penetrated the bamboo channels effectively.[30] Upon the disappearance of internal bubbles, signifying complete solution penetration, the samples were transferred to a controlled environment maintained at 20°C and 60% relative humidity for 12 hours to facilitate the comprehensive deposition of Ag(I) on both the internal and external surfaces of the bamboo.

Both pre-DB and pre-DB-Ag samples were then immersed in a 5% (V/V) solution of stearoyl chloride in toluene and placed in a vacuum chamber at –0.075 MPa for 1 hour to facilitate soaking. The samples were subsequently air-dried in a ventilation cabinet and named pre-DB-Ag-S and pre-DB-S, respectively.

The pre-DB, pre-DB-Ag, pre-DB-S, and pre-DB-Ag-S samples underwent hot pressing at 60°C and 5 MPa for 20 minutes to yield DB, DB-Ag, DB-S, and DB-Ag-S, respectively. To achieve omni-surface hydrophobic bamboo, the DB-Ag-S samples were evenly coated with hard acyl chloride and quickly sprayed, followed by drying in a ventilation cabinet to obtain the SHDB-Ag-S, an omni-surface hydrophobic bamboo product. The distance between the spray bottle and the bamboo surface is generally 15 to 25 cm. The spray bottle should be kept as vertical as possible to the bamboo surface to ensure that the solution can be evenly covered on the surface.

2.4 Structure and characterization

The chemical structures of NB, DB, DB-Ag, DB-S, DB-Ag-S, and SHDB-Ag-S were characterized by Fourier transform infrared spectroscopy (FTIR) and X-ray photoelectron spectroscopy (XPS). Their crystalline structures were analyzed by X-ray diffraction (XRD). The scattered radiation was recorded in a range of 5–90° at a rate of 5°/min. The chemical composition of NB and DB was determined using the National Renewable Energy Laboratory (NREL) method. The microscopic morphology and structure of all samples were analyzed by field emission scanning electron microscopy

Fig. 1: Reaction mechanism of omni-surface hydrophobic bamboo.

(SEM). The samples are sprayed with gold before scanning to improve their electrical conductivity. The thermal properties of NB, DB, DB-Ag, DB-S, DB-Ag-S, and SHDB-Ag-S were analyzed using thermogravimetry (TG) at a rate of 10 ℃/min in a nitrogen atmosphere from 30 ℃ to 800 ℃.

2.5 Surface water wettability analysis

The water contact angle (WCA) measurements for the samples NB, DB, DB-Ag, DB-Ag-S, DB-S, and SHDB-Ag-S, along with the sliding angle (SA) of SHDB-Ag-S, were conducted using an optical contact angle meter. This analysis aimed to evaluate how Ag(I) impregnation and hard acylation influence the surface wettability. The WCA values were derived from the mean of five distinct measurements on each sample. To further assess the dynamic water wettability, 4 μL droplets of deionized water were placed on the bamboo surfaces, with contact angle changes documented every 60 seconds over a 180-second period.

In many industrial and daily applications, the durability of the SHDB-Ag-S samples was divided into 6 groups and placed in different environments (G1-G6), and their contact angles were measured and compared with those of the G0 group (blank group).

G0: Untreated SHDB-Ag-S samples, acting as a control group.

G1: Samples were immersed in deionized water for 48 hours.

G2: Samples were immersed in an HCl solution at pH 1 for 48 hours.

G3: Samples were immersed in a NaOH solution at pH 12 for 48 hours.

G4: Samples were subjected to ultrasonic treatment in deionized water for 1 hour at a frequency of 40 kHz and a power of 100 W.

G5: Samples were exposed to ultraviolet light with a power output of 40 W and a wavelength of 365 nm for a duration of 10 days.

G6: Samples underwent abrasion testing with 120 mesh sandpaper for 50 cycles using a wear testing machine.

2.6 Physical properties of bamboo

To investigate the water resistance and dimensional stability of the bamboo samples, strips were submerged in deionized water at ambient temperature, with their weights and dimensions monitored every 12 hours until they reached a state of dimensional equilibrium. The water uptake (WU) was calculated using Eq. (1):

$$WU\ (\%) = (W_2 - W_1) / W_1 \times 100 \quad (1)$$

where W_1 and W_2 represent the weights of the samples before and after immersion in deionized water, respectively.

Concurrently, the water uptake rate (h) was determined by Eq. (2):

$$\text{Water uptake rate}\ (\%\ /\ h) = WU / \Delta t \quad (2)$$

After 180 hours of immersion, the radial, tangential, and volumetric swelling were measured with a digital micrometer accurate to ± 0.01 mm. The volumetric swelling (S) was then calculated using the Eq. (3):

$$S\ (\%) = (V_2 - V_1) / V_1 \times 100 \quad (3)$$

where V_1 and V_2 are the volumes of the samples before and after immersion in deionized water, respectively.

The water resistance and dimensional stability of the samples were assessed by determining the mean water repellency efficiency (WRE) and anti-swelling efficiency (ASE) with the following Eqs. (4) and (5):

$$WRE\ (\%) = (WU_u - WU_t) / WU_u \times 100 \quad (4)$$

$$ASE\ (\%) = (S_u - S_t) / S_u \times 1 \quad (5)$$

where WU_u and WU_t are the WU of an untreated sample and a treated bamboo sample after water immersion for a certain time, respectively, while S_u and S_t are the S corresponding to WU_u and WU_t, respectively.

2.7 Mildew resistance test

In accordance with the Chinese standard GB/T18261–2013, this study aimed to assess the mildew resistance of NB, DB, DB-Ag, DB-S, DB-Ag-S, and SHDB-Ag-S. The sample size for the mildew test was determined, and the molds *A. niger, T. viride, and P. citrinum* were utilized in the testing, as detailed in a previous study by Yang et al., 2021. The extent of mold infection on the samples was monitored daily. A rating scale of 0 to 4 was employed to denote the percentage of mold coverage on the samples, where 0 signifies the absence of mold, and each increment by 1 on the scale represents an additional 25% of coverage, culminating in 100% at the maximum score of 4.

Employing Eq. (6), we calculated and assessed the mildew resistance capabilities of the high-strength, mildew-resistant bamboo materials:

$$E = (1 - D_1/D_2) \times 100\% \quad (6)$$

where E is the prevention and control effect; D_1 is the average infected area of treated samples; D_2 is the mean infected area of the control sample.

3. Results and discussion

3.1 Chemical composition and structure

The functional groups of NB, DB, DB-Ag, DB-S, DB-Ag-S, and SHDB-Ag-S were studied by FTIR spectroscopy, as shown in Fig. 2a. In the spectrum of SHDB-Ag-S, two strong adsorption peaks appear at 2918 cm^{-1} and 2854 cm^{-1}, which can be attributed to the asymmetric stretching vibration of $–CH_3$ and the symmetric stretching vibration of $–CH_2$ in the long alkyl chain of stearoyl chloride.[25] A new carbon–based signature peak appeared at 1700 cm^{-1}, indicating that stearyl chloride was successfully attached to the bamboo cell wall via ester bonds.[31] Compared to SHDB-Ag-S and DB-Ag-S, these peaks were heightened in the spectrum of SHDB-Ag-S, which

proved that stearoyl chloride has been loaded onto the bambo by spraying. The absorption peaks at 1560, 1515, and 1249 cm^{-1} were weakened significantly in the DB spectrum, which indicates that the lignin was largely removed.[32] In addition, the –OH tensile peak at 3419 cm^{-1} was enhanced after stearoyl chloride treatment, indicating that stearoyl chloride treatment had a great effect on the hydrogen bonding of bamboo, and there was hydrogen bonding between stearoyl chloride and bamboo.[33]

The chemical composition of NB and DB was analyzed using high-performance liquid chromatography (HPLC), as illustrated in Table.1. NB was found to contain 54.77% cellulose, 14.68% hemicellulose, and 25.68% lignin. Following the alkali treatment process, the composition of DB changed significantly: the lignin content was reduced from 25.68% to 19.29%, the hemicellulose content decreased from 14.68% to 10.46%, and the cellulose content increased from 54.77% to 61.18%. This indicates that the alkali treatment partially removed hemicellulose and lignin components.[34]

Fig. 2b presents the X-ray diffraction patterns for NB, DB, DB-Ag, DB-S, DB-Ag-S, and SHDB-Ag-S. The unmodified NB and the lye-treated DB display similar diffraction profiles,characterized by three distinct peaks at 2θ angles of 15.93°, 22.24°, and 34.60°. These peaks are associated with

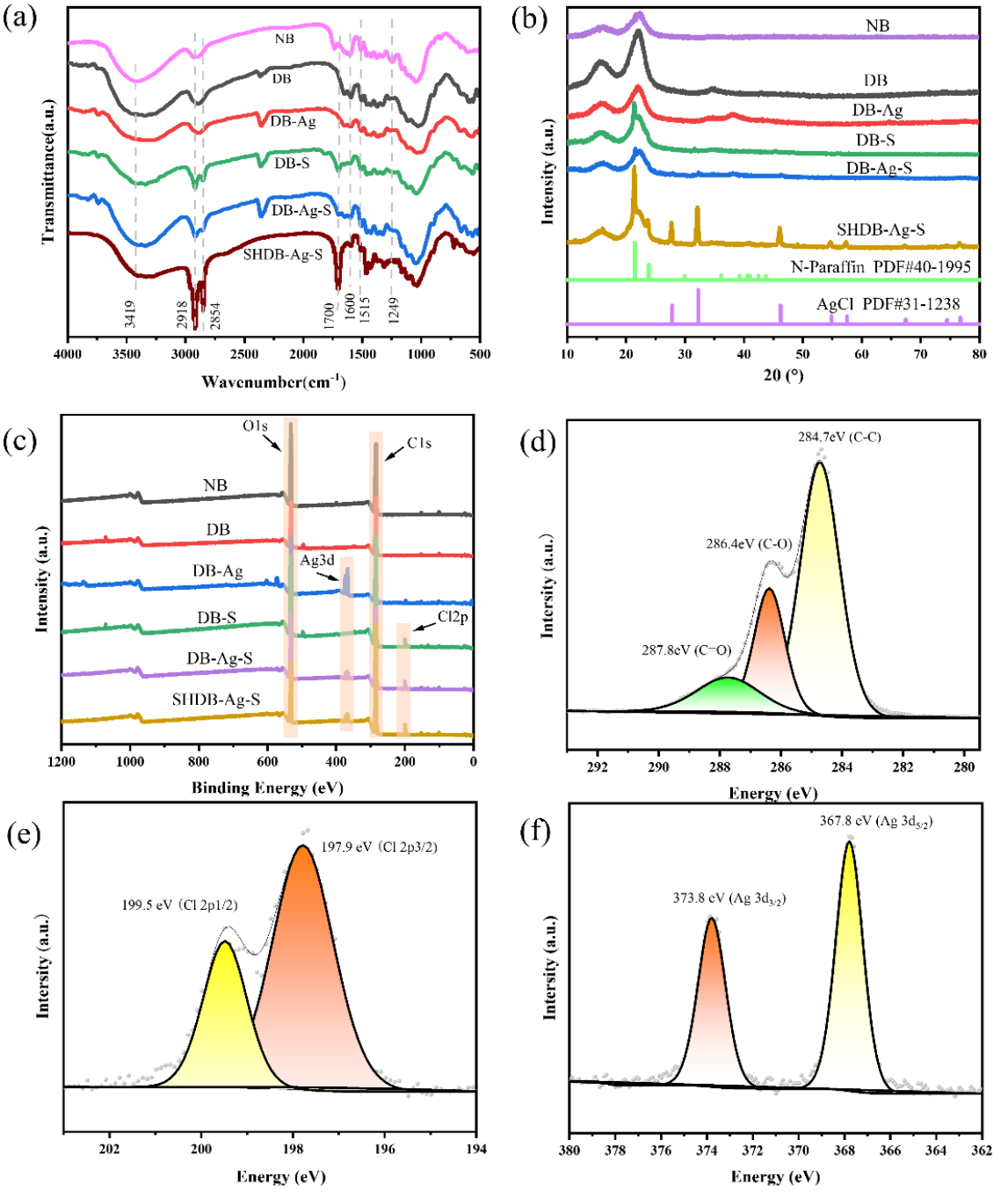

Fig. 2: FTIR spectra (a); XRD spectra (b); XPS, NB, DB, DB-Ag; DB-Ag-S and DB-S (c); the wide sweep spectrum; C1s core-level of SHDB-Ag-S (d); Cl2p core-level of SHDB-Ag-S (e); Ag3d core-level of SHDB-Ag-S (f).

Table 1: Chemical composition of bamboo (% dry matter).

Samples	Cellulose (%)	Hemicellulose (%)	Lignin (%)
NB	54.77	14.68	25.68
DB	61.18	10.46	19.29

the (110), (002), and (004) crystallographic planes of cellulose, respectively.[35] The findings revealed an increase in the crystallinity index (CrI) of cellulose from 53.16% in NB to 57.95% in DB. This enhancement in CrI is due to the removal and partial removal of hemicellulose and lignin through alkali treatment, which leads to a reorganization of the crystal structure and a relative decrease in the amorphous region content.[36] Additionally, eight new diffraction peaks appeared at 27.8°, 32.2°, 46.2°, 54.8°, 57.5°, 67.5°, 74.5°, and 76.7° for the c phase, corresponding to the (111), (200), (220), (311), (222), (400), (331), and (420) crystallographic planes of AgCl (PDF card 31–1238), respectively. The SHDB-Ag-S displayed additional peaks at 2θ angles of 21.5°, 23.9°, 29.9°, 36.1°, 39.2°, 40.6°, 41.1°, 42.5°, and 43.8°, which are associated with the (110), (200), (210), (020), (011), (310), (111), (201), and (220) diffraction peaks from N-Paraffin (PDF card 40–1995). As anticipated, the XRD pattern of SHDB-Ag-S showed the coexistence of diffraction peaks from both AgCl and N-paraffin, indicating the presence of AgCl NPs and long alkyl chains from stearoyl chloride within the SHDB-Ag-S. This observation is consistent with the results obtained from FTIR, XPS, and SEM.

The surface element state and chemical composition of modified bamboo were further determined by XPS analysis. As shown in Fig. 2c, the characteristic peaks of C, Cl, and Ag can be observed. In addition, the XPS high-resolution curve of SHDB-Ag-S is shown by peak-splitting fitting in Fig. 2e–f. In the XPS spectrum of C1s shown by Fig. 2d, the three peaks at 284.7, 286.4, and 287.8 eV correspond to the C–C/C–O signal and the C=O signal, respectively.[37] Besides, the high-resolution XPS spectra of Cl2P3/2 and Cl2P1/2 in Fig. 2e showed that the binding energies were 197.9 eV and 199.5 eV, respectively.[38] Two shake-up satellites for Cl2P1/2 and Cl2P3/2 were also detected, resulting in a spin energy difference of 1.6 eV, confirming the formation of the chloride. The high-resolution XPS spectra of Ag in Fig. 2f showed that the binding energies of Ag3d5/2 and Ag3d3/2 were 367.8 eV and 373.8 eV.[39] In addition, two shake-up satellites for Ag3d3/2and Ag3d5/2 were also detected, resulting in a spin energy difference of 6.0 eV, confirming the formation of the halides. Notably, the peak intensities of C1s and O1s in DB are lower than in NB, which is due to the partial removal of hemicellulose.[40] And the peak intensities of Ag3d in DB-Ag-S were lower than those of DB-Ag, which may be caused by the introduction of stearyl chloride as an organic component.

3.2 Fabrication process and reaction mechanism

In this research, omni-surface hydrophobic bamboo SHDB-Ag-S was prepared by liquid deposition, hot pressing, and the spray method. The reaction mechanism is shown in Fig. 1; cellulose molecules contain multiple hydroxyl groups (–OH).[41] When dissolved in water, silver nitrate forms Ag (I), which forms a coordination bond with the hydroxyl group on the cellulose, resulting in the hydrogen on the hydroxyl group on the cellulose being replaced by Ag(I).[42] Stearyl chloride is a commonly used organic acylation reagent, which can esterify the hydroxyl group in cellulose.[43] The acyl chloride (–COCl) in stearyl chloride is a good leaving group and can be replaced by the cellulose hydroxyl group (–OH) in the reaction. Stearyl chloride can react with cellulose in bamboo to produce cellulose stearate, a robust hydrophobic compound. This reaction facilitates the omni-surface hydrophobic modification of bamboo.[44] This provides the conditions for the omni-surface hydrophobic modification of bamboo.

The bamboo prepared under six different conditions (NB, DB, DB-Ag, DB-Ag-S BD–S, SHDB-Ag-S) was characterized by scanning electron microscopy, and the changes of its surface morphology were observed, as shown in Fig. 3a. After pretreatment, the gap between DB Fig. 3a2 fibers increased, providing an active site for Ag(I) loading. DB-Ag Fig. 3a3 can clearly observe many nanoparticles attached to the bamboo surface.[45] SEM images of bamboo sections showed that NB Fig. 3b1 cell cavities were round and full, and DB Fig. 3b2 cell walls collapsed after pretreatment. The collapse of the cell wall is attributed to the partial removal of hemicellulose and lignin, which are crucial components of the cell wall, during the pretreatment process.[46] In Figs. 3b4-b5, it can be obviously observed that the pores between bamboo cells of DB-Ag-S and DB-S are filled with stearoyl chloride. The layered structure of SHDB-Ag-S is shown in Fig. 3b6, which is a flat particle formed by rapid cooling and solidification after the molten chlorine stearate particles hit the bamboo at high speed during the spraying process.[47] These particles accumulate layer by layer to form a coating with a typical layered structure.[48] EDS element mapping and energy-dispersive X-ray (EDX) spectroscopy were used to confirm the successful loading of Ag. As shown in Figs. 3c2-c6, it can be clearly observed that C, N, O, Ag, and Cl elements are evenly distributed on the surface of bamboo SHDB-Ag-S. As shown in Fig. 3d, the peak of Ag element in the sample SHDB-Ag-S can be observed, and the mass fraction of Ag element is 3.41%, which further determines the loading of Ag.

3.3 Thermal properties of composites

Fig. 4h1 and Fig. 4h2 show the TGA-DTG curves of NB, DB, DB-Ag, DB-S, DB-Ag-S, and SHDB-Ag-S. The initial weight loss before 100 °C is caused by the evaporation of water in the bamboo. The 100 to 380 °C range is the main mass loss area

for cellulose, hemicellulose, and lignin in bamboo.[49] The mass loss observed in the 160-280 ℃ range may be associated with the incomplete degradation of stearoyl chloride. The 380–600℃ range represents the carbonization zone, where further degradation of L-glucose occurs, leading to the formation of low molecular weight products.[50] The final residual mass in the TGA and DTG diagrams is 14.89% (NB), 26.98% (DB), 22.95% (DB-Ag), 22.13% (DB-S), 19.19% (DB-Ag-S), and 18.85% (SHDB-Ag-S), respectively.

3.4 Surface wettability, water repellency and dimensional stability

The WCA test results of the composite material are shown in Fig. 4a. Natural bamboo has a strong hydrophilicity, with an outer surface WCA of 55.77° and an inner surface WCA of 51.07°. When the water drops on the surface of natural bamboo, the water droplets are rapidly absorbed by naturalbamboo, and the WCA drops to 0° at the inner and outer surfaces in 60 s. After $AgNO_3$ impregnation, the outer surface

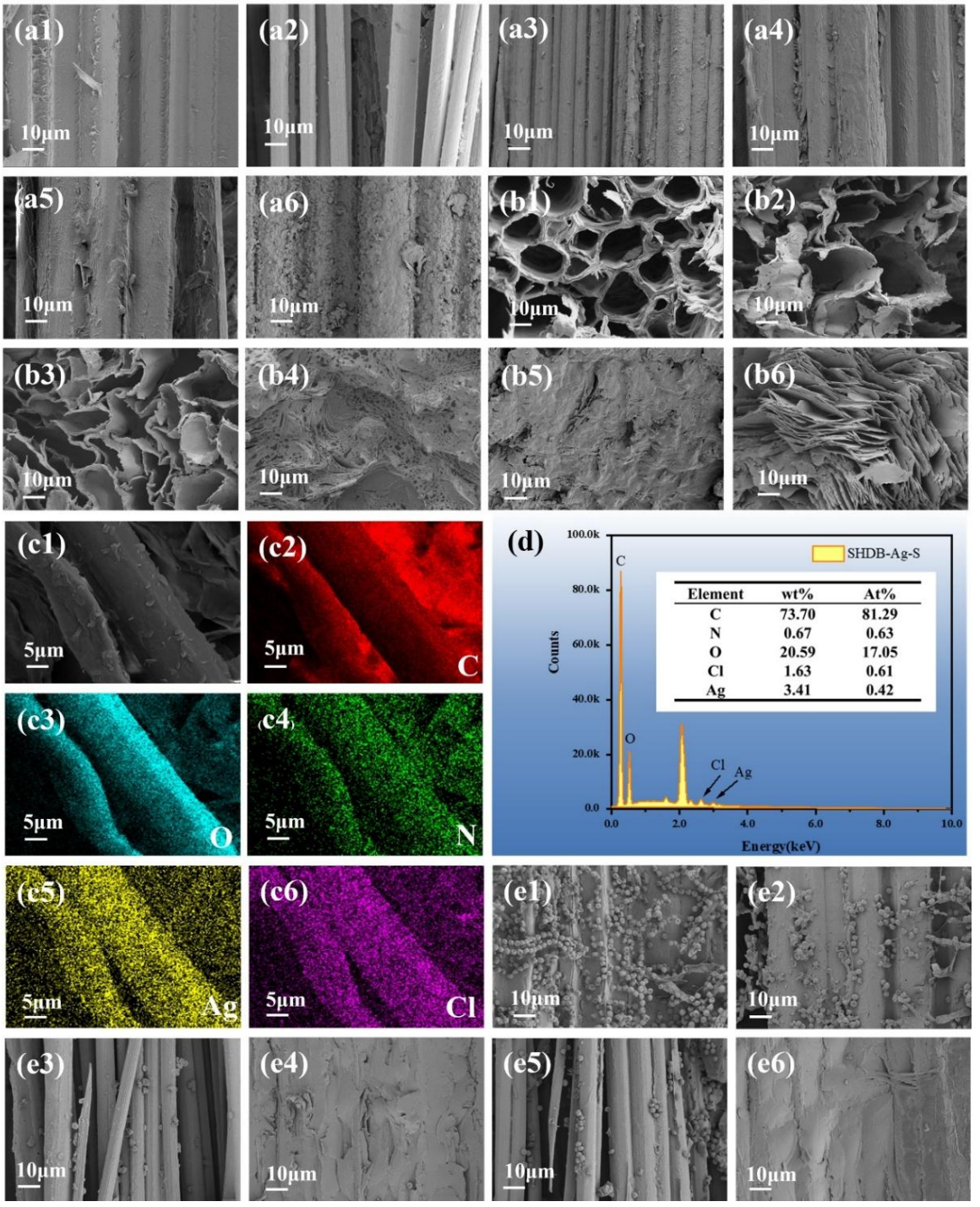

Fig. 3: SEM images (a-surface, b-cross-section) of NB (a1, b1), DB (a2, b2), DB-Ag (a3, b3), DB-Ag-S (a4, b4), DB-S (a5, b5), SHDB-Ag-S (a6, b6). EDS mapping images of SHDB-Ag-S (d) (c2:C, c3:O, c4: N, c5: Ag, c6: Cl); the SEM images (e) of the sample infected by mold.

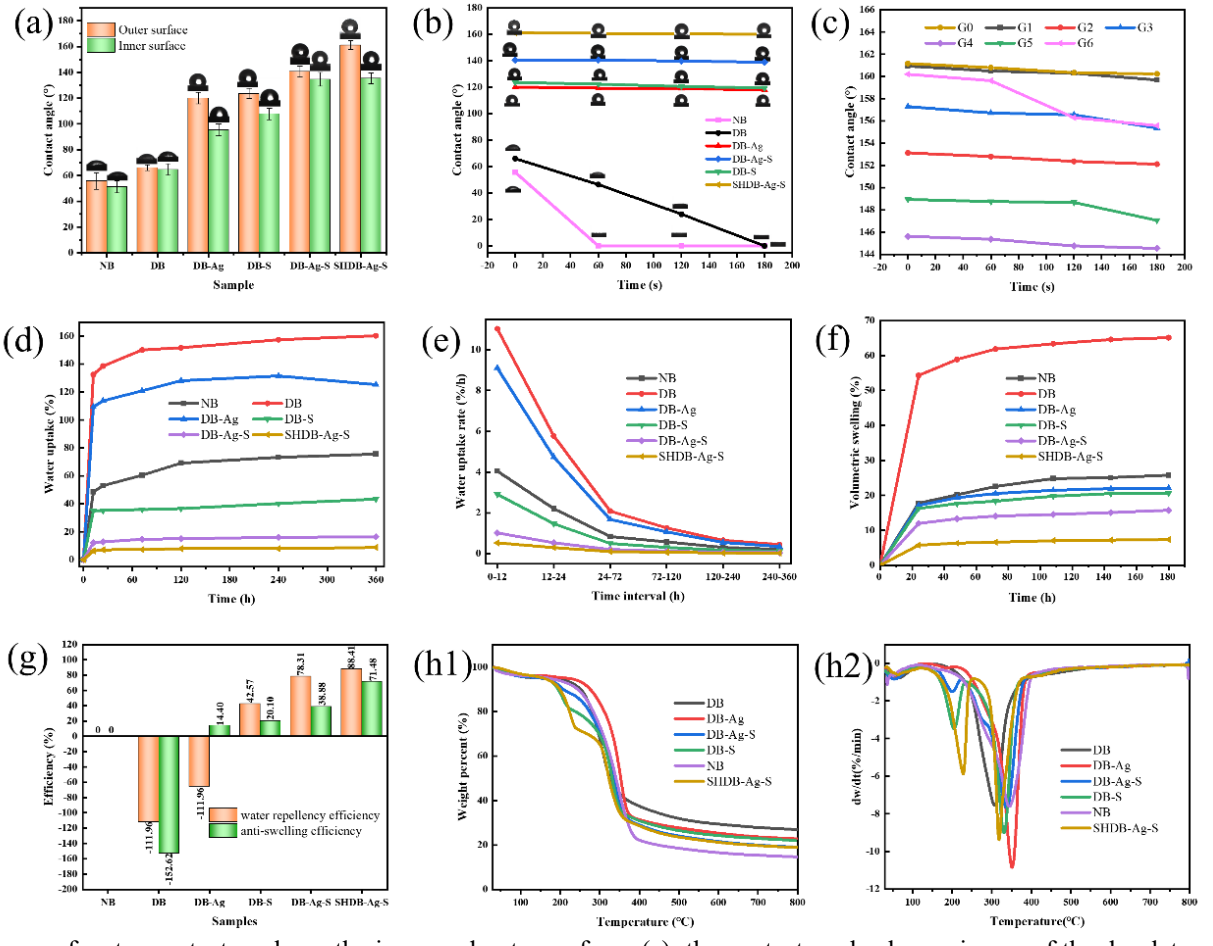

Fig. 4: Image of water contact angle on the inner and outer surfaces (a); the contact angle change image of the droplet resting (b); image of contact angle change within 180s after the SHDB-Ag-S durability test (c); water uptake (d), water uptake rate (e), volumetric swelling (f), water repellency efficiency, and anti-swelling efficiency (g); the TG (h1) and DTG (h2) curves of NB, DB, DB-Ag, DB-S, DB-Ag-S, and SHDB-Ag-S.

WCA of DB-Ag increased to 120.10° and the inner surface WCA increased to 95.34°. Through the $AgNO_3$ impregnation process, Ag(I) ions were successfully introduced into the bamboo's microporous network. Subsequent reaction with NaOH solution induced the formation of Ag_2O deposits, which were preferentially localized within the internal voids and on the external surfaces of the bamboo.[51] This surface modification process contributed to the enhanced roughness observed on both the interior and exterior regions of the bamboo matrix. Surface roughness is an important factor affecting hydrophobicity, and the hydrophobicity of a surface can be enhanced by increasing roughness.[52] Following the grafting of stearyl chloride, the water contact angle (WCA) of DB-S rose to 123.67° on the outer surface and 107.78° on the inner surface. This increase in WCA is attributed to the long-chain alkyl groups present in the hard acyl chloride, which lower the surface energy of the bamboo. Consequently, the reduced surface energy contributes to the enhanced hydrophobicity of the bamboo material.[53]

Furthermore, when stearyl chloride and Ag(I) were introduced simultaneously, the water contact angle (WCA) on the outer surface of DB-Ag-S increased to 140.59°, and the inner surface WCA rose to 134.63°. These findings indicate that both the augmentation of surface roughness and the reduction of surface energy can significantly elevate the WCA values. However, the SHDB-Ag-S, which was treated with a superhydrophobic surface spray, demonstrated exceptional hydrophobic characteristics across all areas, with an outer surface WCA of 161.16°, an inner surface WCA of 135.47° (as shown in Fig. S1), and a sliding angle of 8° (as depicted in Fig. S5c). During the experimental observations, it was noticeable that water droplets on the bamboo surface did not penetrate but instead exhibited a propensity to roll off.[54] The WCA images of droplets remaining on the surfaces of NB, DB, DB-Ag, DB-S, DB-Ag-S, and SHDB-Ag-S for 180 seconds are presented in Fig. 4b. The outer surface WCA of NB plummeted from 55.77° to 0° within a minute, marking it as the least hydrophobic. In contrast, the outer surface WCA of SHDB-Ag-S only slightly decreased from 161.16° to 160.23° over 180 seconds, suggesting that water droplets could not readily infiltrate the interior of SHDB-Ag-S, thereby highlighting its superb overall surface hydrophobicity. This superhydrophobic quality endows bamboo with self-cleaning capabilities. Photographs illustrating the self-cleaning properties of SHDB-Ag-S are provided in Fig. S2 and Videos 1 and 2.

In many industrial and daily applications, the durability of the superhydrophobic layer on the material surface is a key factor determining the service life of the material. In order to test the durability of superhydrophobic surfaces, the SHDB-Ag-S samples were divided into 6 groups and placed in different environments (G1-G6), and their contact angles were measured and compared with those of the G0 group (blank group). After 6 groups of tests, WCA within 180 s was measured, and the results were shown as follows (Fig. 4c): G1 had almost no effect on the surface hydrophobicity of SHDB-Ag-S, while G4 had the greatest effect on the surface hydrophobicity of SHDB-Ag-S, which may be caused by ultrasonic cleaning away part of the stearoyl chloride coating.[55] The six sets of tests may simulate different environmental conditions, such as pH changes, UV aging, and mechanical friction, which can fully assess the challenges that superhydrophobic layer may encounter in practical use. Even after several tests, the surface contact angle of SHDB-Ag-S remains at a very high level, which indicates that its hydrophobic layer has good chemical and physical stability and is not easily destroyed or stripped. Comprehensive testing allows for a thorough understanding of the performance of superhydrophobic layer under various environmental conditions encountered in actual use, thereby ensuring its reliability and durability for its intended applications.

To evaluate the water uptake of NB, DB, DB-Ag, DB-S, DB-Ag-S, and SHDB-Ag-S, the samples were submerged in deionized water for a duration of 360 hours, with the experimental outcomes displayed in Fig. 4d and Fig. S3. As depicted in Fig. 4e, all samples exhibited similar patterns of water absorption. Notably, the initial 24 hours saw a rapid increase in water absorption across all samples, after which the rate of absorption progressively slowed. After a 360-hour period, the water uptake of DB reached 75.57%, whereas SHDB-Ag-S recorded a significantly lower uptake of only 8.76%. The removal of certain non-cellulosic components during treatment exposes a multitude of hydroxyl groups in the cellulose, rendering DB more hydrophilic, which is the primary reason for its substantial water uptake of 160.19%.[35] The soaking process for NB and SHDB-Ag-S is illustrated in

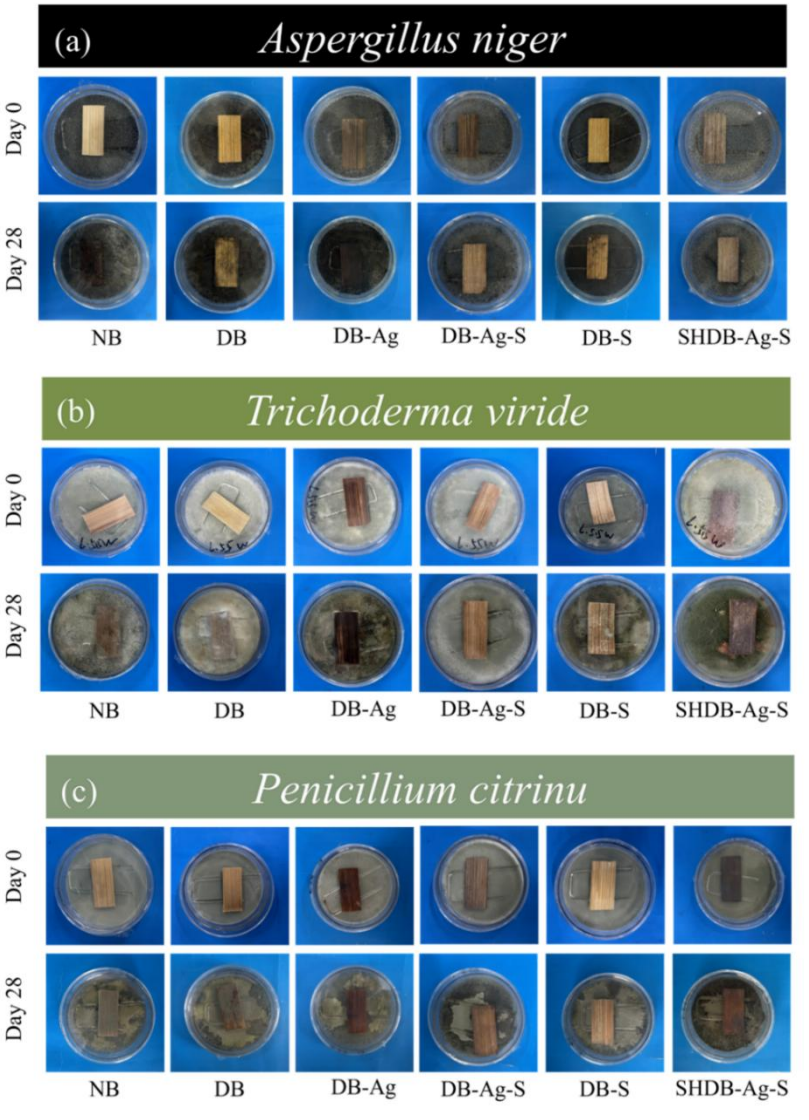

Fig. 5: Sample before and after mold infection.

Fig. S4. It is evident that NB displayed a pronounced wicking phenomenon after being immersed in water, whereas SHDB-Ag-S remained completely non-wettable. The water uptake of the omni-surface hydrophobic bamboo was reduced by 88.41% compared to that of natural bamboo, dropping from 75.57% to 8.76%. Furthermore, Figs. 4f-g presents the volumetric swelling coefficient and anti-swelling efficiency of the bamboo before and after treatment. The average volumetric swelling for NB and SHDB-Ag-S was 25.77% and 7.35%, respectively, with corresponding anti-swelling efficiency values of 0% and 71.48%. The water repellency efficiency of SHDB-Ag-S saw an increase from 0% to 88.41% when compared to the original bamboo. These findings indicate that the omni-surface hydrophobic bamboo significantly enhances the dimensional stability of the material.

3.5 Anti-mildew performances

Fig. 5 is a photo of samples tested for 28-day mildew protection against *A. niger*, *T. viride*, and *P. citrinum.* As shown in Fig. 6, NB were infected by *A. niger, T. viride,* and *P. citrinum* on the 3rd day. On the 9th day, the area of NB infected with *A. niger*, *T. viride,* and *P. citrinum* was more than 75%, and the infection grade was 4, suggesting that they are very poorly resistant to *A. niger*, *T. viride*, and *P. citrinum*. Because bamboo is not only nutritious, it is also very hygroscopic, which provides conditions for the growth of mold. Whereas DB was not infected by *A. niger* over the first 2 days, hyphae appeared on the surface on the 3rd. After 28 days, the infection grading values were 3, with only 60% of the area infected, as shown in Fig. 5a and Fig. 6a2. This means that DB had an antifungal effect, and the growth of *A. niger*

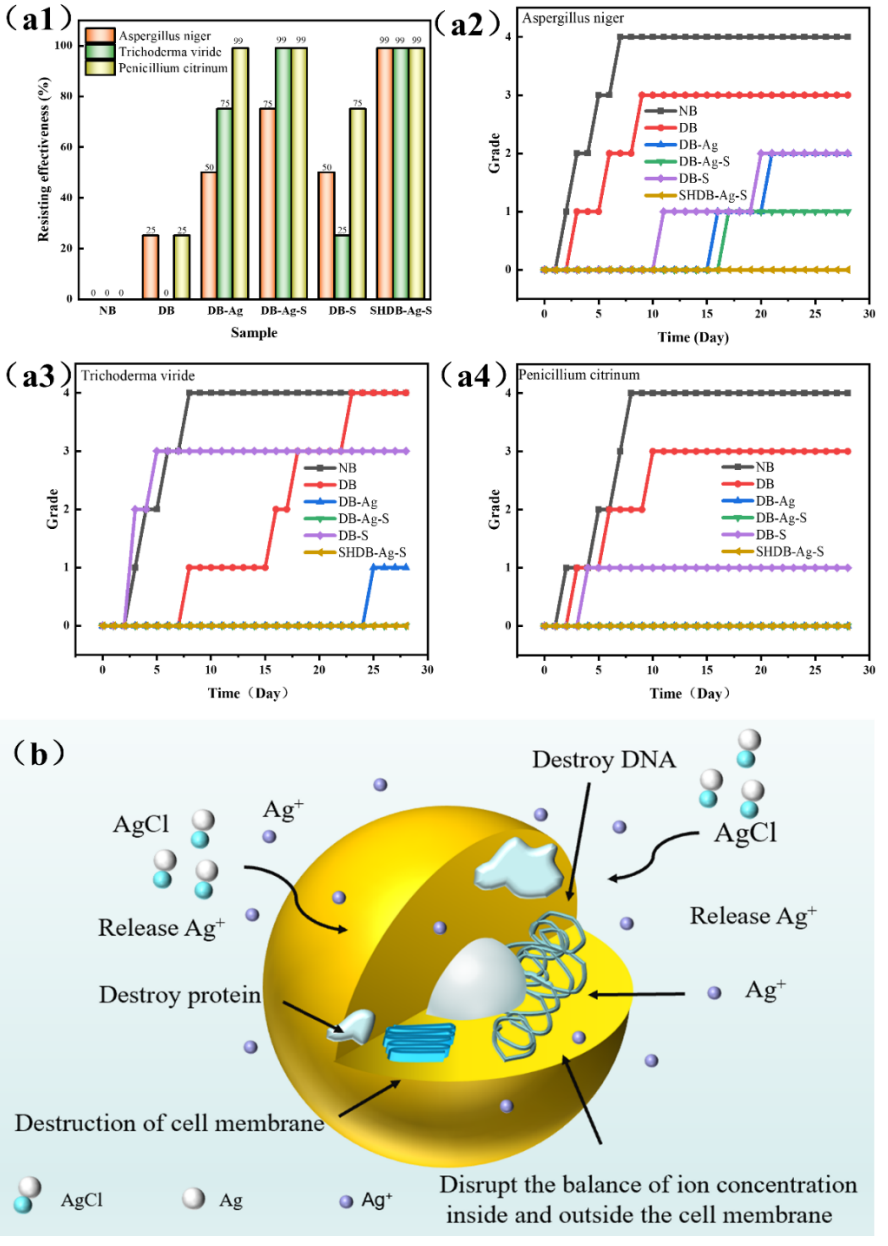

Fig. 6: Mold control efficacy (a) of NB, DB, DB-Ag, DB-Ag-S, SHDB-Ag-S, and DB-S samples infected by mold were obtained; the control grade of the sample against mold of *A. niger* (a2), *T. viride* (a3), and *P. citrinun* (a4); the anti-mildew mechanism of AgCl NPs (b).

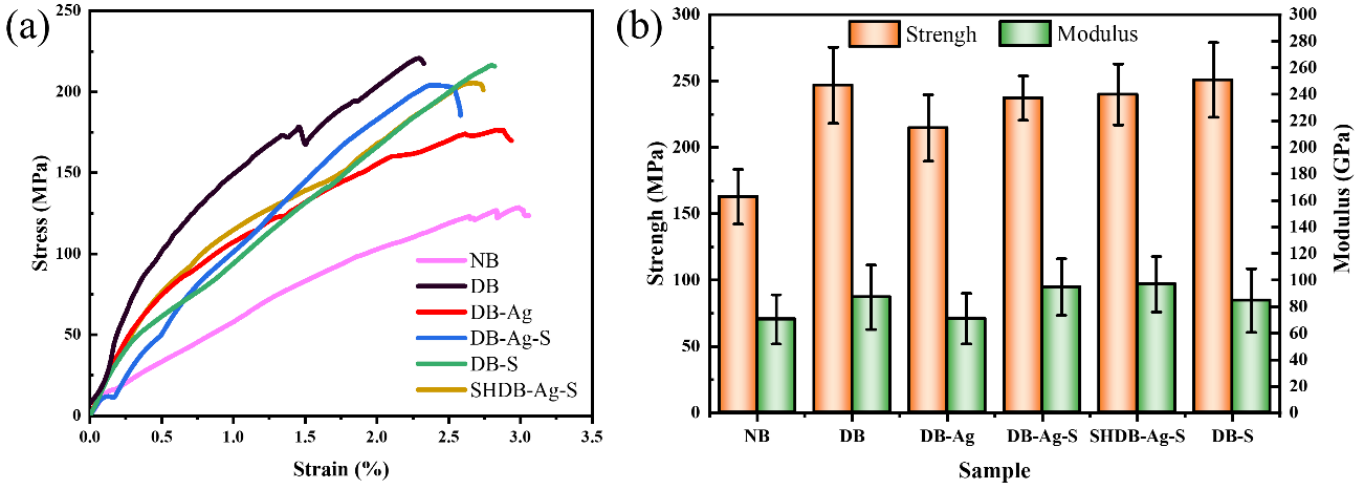

Fig. 7: Stress-strain curve (a) and the tensile strength and tensile modulus (b) of NB, DB, DB-Ag, DB-Ag-S, DB-S and SHDB-Ag-S.

was inhibited. It was attributed to the partial removal of nutrients such as hemicellulose and the collapse of bamboo parenchyma cells to form interlocking structures after alkali treatment.[56] Whereas DB-Ag, DB-S, and DB-Ag-S were not infected by *A. niger* over the first 10 days, hyphae appeared on the surface on the 17th, 11th, and 18th days, respectively. After 28 days, the infection grading values were 2, 2, and 1, with only 30%, 30%, and 10% of the area infected, respectively (Fig. 5a and Fig. 6a2). This means that DB-Ag, DB-S, and DB-Ag-S had antifungal effects, and the growth of *A. niger* was significantly inhibited. Ag(I) can be slowly released by elemental silver and silver oxide.[57] Ag(I) has high biological activity and can interact with proteins and enzymes on the cell membrane of microorganisms, destroying the integrity of the cell membrane and causing the cell contents to leak, thereby inhibiting or killing microorganisms.[58] During the 28-day observation, no *A. niger*, *T. viride*, or *P. citrinum* was found on the surface of SHDB-Ag-S (Fig. 5 and Fig. 6a). Fig. 3e is the SEM image of the sample infected by mold 28 days later. The surface of NB Fig. 6b was fully covered with mycelia and spores, while the surface of SHDB-Ag-S remained clean and uninfected by mold. The anti-mildew efficacy of SHDB-Ag-S against three kinds of mold was greater than 99%. The superhydrophobic surface is not easy to moisten with water, which reduces the retention of water on the surface of the material and provides an unfavorable environment for mold growth.[59] The special structure and chemical properties of the omni-surface hydrophobic can inhibit the attachment and growth of mold. Neither DB-Ag nor DB-S could achieve greater than 99% of the control efficacy of the three molds, but the superhydrophobic modified SHDB-Ag-S could achieve greater than 99% of the control efficacy of the three molds, indicating that loaded silver and stearyl acylation modification had a synergistic effect on the control of mold.

3.6 Mechanical strength of composites

Figs. 7a and b describe the typical stress-strain curves of NB, DB, DB-Ag, DB-Ag-S, SHDB-Ag-S, and DB-S with the corresponding tensile strength and Young's modulus. As shown in Fig. 7a, compared with other bamboo materials, DB-S has the highest tensile strength of 250.79 MPa and its tensile modulus is 84.63 GPa. After adding Ag(I), the tensile strength and Young's modulus of DB-Ag decreased to 214.58MPa and 71.02 GPa respectively due to the destruction of hydrogen bond between fibers.[50] The esterification reaction may enhance the interaction between stearyl chloride and bamboo fiber, such as hydrogen bonding, which increased the stress of the composite bamboo and increased the tensile strength and Young's modulus of DB-Ag-S to 237.023MPa and 94.82 GPa, respectively. Compared with untreated natural bamboo, the tensile strength and Young's modulus of the SHDB-Ag-S increased to 239.83MPa and 96.83 GPa, respectively.

4. Conclusion

An omni-surface hydrophobic bamboo composite (SHDB-Ag-S) exhibiting superior properties was effectively synthesized through a combination of liquid deposition, hot-pressing, and spraying techniques. The inhibitory effect of SHDB-Ag-S on A. niger, T. viride and P. citrinum orange is all greater than 99%, while natural bamboo has no inhibitory effect on mold. Stearyl chloride spraying further enhances the superhydrophobicity of bamboo. The water contact Angle on its outer surface is 161.16°, which is 2.89 times that of natural bamboo (55.77°), and the water contact Angle on its inner surface is 135.47°; the sliding angle is 8°. The improvement of hydrophobicity further enhances the dimensional stability of bamboo materials. The water repellency and anti-expansion rate of SHDB-Ag-S have increased to 88.41% and 71.48% respectively. The tensile strength of SHDB-Ag-S is 1.47 times that of natural bamboo and its Young's modulus is 1.37 times that of natural bamboo. Omni-surface hydrophobic bamboo composite (SHDB-Ag-S) can be used in interior decoration, furniture boards and bamboo handicrafts, *etc*., and has extensive and diverse application prospects.

Acknowledgments
This work was supported by the National Natural Science Foundation of China (No. 31971741, 32160414), the Yunnan Fundamental Research Projects (No. 2018FB066, No. 202001AT070141), and Yunnan Agricultural Basic Research Special Projects (No. 202101BD070001-086). The authors extend their appreciation to the Deanship of Scientific Research at Northern Border University, Arar, KSA, for funding this research work through the project number NBU-FFR-2025-2193-22.

Conflict of Interest
There is no conflict of interest.

Supporting Information
Applicable.

References
[1] A. Seilkhan, An Overview of Green Applications of Natural Products for Pharmaceutical, Biofuel, and Rubber Industries: Case Study of Kazakh Dandelion (Taraxacum kok-saghyz Rodin), *ES Energy & Environment*, 2024, **25**, 1171, doi: 10.30919/esee1171.

[2] N. Zhakiyev, N. Sagadatova, G. Ismagulova, A. Bakdolotov and A. Biloshchytskyi, Hybrid Technico-Economical Modeling of the Mid-Term Green Economy and Low-Carbon Development Strategy of Kazakhstan, *ES Energy & Environment*, 2024, **25**, 1235, doi: 10.30919/esee1235.

[3] A. Kaur, M. V. Singh, N. Bhatt, S. Arora A. Shukla, Exploration of Chemical Composition and Biological Activities of the Essential Oil from Ehretia acuminata R. Br. Fruit, *ES Food & Agroforestry*, 2024, **15**, 1068, doi: 10.30919/esfaf1068.

[4] Y. Zhang, M. Bai, A. Zhang, X. Zhang, Y. Dong, H. Kang, Q. Zhang, J. Li, A facile and small-molecule regulated borate network gelation to improve the mildew proof, fire-retardant of bamboo. *Industrial Crops and Products*, 2023, **197**, 116602. doi: 10.1016/j.indcrop.2023.116602.

[5] S. Gajbhiye, M. Salve, M. Gaikwad, A. Rasage, M. Khater, V. Ghadage, N. Chaure, Influence of synthesis conditions on the physical characteristics and antibacterial activities of cerium oxide nanoparticles in biomedical applications, *Engineered Science*, 2024, **32**, 1254, doi: 10.30919/es1254.

[6] M. Ruzi, N. Celik, F. Sahin, M. Sakir, M. Onses, Nanostructured Surfaces with Plasmonic Activity and Superhydrophobicity: Review of Fabrication Strategies and Applications, *Small*, 2025, **21**, 2408189, doi: 10.1002/smll.202408189.

[7] W. Huang, J. Huang, Z. Guo, W. Liu b, Icephobic/anti-icing properties of superhydrophobic surfaces, *Advances in Colloid and Interface Science,* 2022, **304**, 102658, doi: 10.1016/j.cis.2022.102658.

[8] Y. Xu, Q. He, F. Zhang, M. Ning, B. Shi, P. Li, Y. Jia, F. Zhang, Preparation and properties of a simple super-hydrophobic carbon fiber composite surface, *Journal of Applied Polymer Science*, 2024, **141**, e55087, doi: 10.1002/app.55087.

[9] Y. Cao, Y. Lu, N. Liu, Y. Li, P. Wang, C. Dai, Y. Wei, Multi-applicable, durable superhydrophobic anti-icing coating through template-method and chemical vapor deposition, *Surfaces and Interfaces*, 2022, **32**, 102100, doi: 10.1016/j.surfin.2022.102100.

[10] F. Liu, P. Li, H. An, P. Peng, B. McLean, F. Ding, Achievements and Challenges of Graphene Chemical Vapor Deposition Growth, *Advanced Functional Material*, 2022, **32**, 2203191, doi: 10.1002/adfm.202203191.

[11] E. Modan, Adriana G. Plăiașu, Advantages and disadvantages of chemical methods in the elaboration of nanomaterials, *The Annals of "Dunarea de Jos" University of Galati*, 2020, **43**, 53-60, doi: 10.35219/mms.2020.1.08.

[12] Q. Jiang, P. Tang, W. Chen, J. Han, R. Wu, Chunming Zhang a b Fabrication and characterization of a novel superhydrophobic cotton fabric with integrated 3D graphene-Ag/TiO2 aerogel for superior antibacterial performance, oil-water separation, and enhanced durability, *Industrial Crops and Products*, 2024, **222**, 119882, doi: 10.1016/j.indcrop.2024.119882.

[13] Y. Tan, K. Fang, W. Chen, Q. Shi, C. Zhang, Fabrication of a superhydrophobic cotton fabric with efficient antibacterial properties and asymmetric wettability via synergistic effect of quaternized chitosan/TiO_2/Ag, *Industrial Crops and Products*, 2024, **209**, 118034, doi: 10.1016/j.indcrop.2024.118034.

[14] Y. Lu, Y. Wu, J. Yang, X. Zhu, F. Sun, L. Li, Z. Shen, Y. Pang, Q. Wu, H. Chen, Gentle fabrication of colorful superhydrophobic bamboo based on metal-organic framework, *Journal of Colloid and Interface Science*, 2021, **593**, 41-50, doi: 10.1016/j.jcis.2021.03.022.

[15] M. Guan, Y. Li, X. Xu, R. Fu, Anti-mold and hydrophobicity of cutinized bamboo prepared via different annealing processes, *Industrial Crops and Products*, 2022, **187**, 115399, doi: 10.1016/j.indcrop.2022.115399.

[16] B. Sun, J. Li, Y. Guo, H. Li, H. Mi, B. Dong, C. Liu, C. Shen, Superhydrophobic UHMWPE Foams with High Mechanical Robustness and Durability Fabricated by Supercritical CO2 Foaming, *ACS Sustainable Chemistry & Engineering*, 2021, **9**, 12663-12673, doi: 10.1021/acssuschemeng.1c04573.

[17] P. Kang, Y. Zhao, T. Wei, Y. Cai, B. Ji, O. Addo-Bankas, Interactions between MPs and PFASs in aquatic environments: A dual-character situation, *Journal of Environmental Management*, 2024, **351**, 119907, doi: 10.1016/j.jenvman.2023.119907.

[18] S. Gonkowski, V. Ochoa-Herrera, Poly- and perfluoroalkyl substances (PFASs) in amphibians and reptiles – exposure and health effects, *Aquatic Toxicology*, 2024, **270**, 106907, doi: 10.1016/j.aquatox.2024.106907.

[19] H. Y. Erbil, Practical Applications of Superhydrophobic Materials and Coatings: Problems and Perspectives, *Langmuir*, 2020, **36**, 2493-2509, doi: 10.1021/acs.langmuir.9b03908.
[20] Z. Tang, T. Tian, P. Molino, A. Skvortsov, D. Ruan, J. Ding, Y. Li, Recent Advances in Superhydrophobic Materials Development for Maritime Applications, *Advanced science*, 2024, **16**, 2308152, doi: 10.1002/advs.202308152.
[21] D. Fu, H. Zheng, W. Sheng, X. Hao, X. Zhang, S. Chang, M. Song, An experimental study on the influence of humidity on ice adhesion strength on superhydrophobic surfaces with microstructures, *Applied Thermal Engineering*, 2024, **244**, 122732, doi: 10.1016/j.applthermaleng.2024.122732.
[22] T. P. Rasitha, N. G. Krishna, B. Anandkumar, S. C. Vanithakumari, J. Philip, A comprehensive review on anticorrosive/antifouling superhydrophobic coatings: Fabrication, assessment, applications, challenges and future perspectives, *Advances in Colloid and Interface Science*, 2024, **324**, 103090, doi: 10.1016/j.cis.2024.103090.
[23] N. Su, C. Fang, H. Zhou, T. Tang, S. Zhang, B. Fei, Hydrophobic treatment of bamboo with rosin, *Construction and Building Materials*, 2021, **271**, 121507, doi: 10.1016/j.conbuildmat.2020.121507.
[24] X. Wang, L. Cao, Y. Hu, Y. Chen, T. Jin, J. Huang, X. Zhang, S. Lin, Highly transparent, hydrophobic, hard and flexible coatings based on a novel melamine-formaldehyde resin synthesized by hydrophobic melamine, *Progress in Organic Coatings*, 2023, **179**, 107487, doi: 10.1016/j.porgcoat.2023.107487.
[25] M. Mirzaaghaei, A. Nasirpour, J. Keramat, S. Goli, M. Dinari, S. Desobry, A. Durand, Chemical modification of waxy maize starch by esterification with saturated fatty acid chlorides: Synthesis, physicochemical and emulsifying properties, *Food Chemistry*, 2022, **393**, 133293, doi: 10.1016/j.foodchem.2022.133293.
[26] A. Erfani, M. Pirouzifard, S. Pirsa, Photochromic biodegradable film based on polyvinyl alcohol modified with silver chloride nanoparticles and spirulina; investigation of physicochemical, antimicrobial and optical properties, *Food Chemistry*, 2023, **411**, 135459, doi: 10.1016/j.foodchem.2023.135459.
[27] M. Chheng, S. Jafari, S. Mehta, D. Mishra, K. Assatarakul, Ultrasound-Assisted Extraction of Bioactive Compounds from Sesbania Javanica Flower: Phenolic Composition, *ES Food & Agroforestry*, 2025, doi: 10.30919/faf1434.
[28] H. Irvani, H. Mahabadi, A. Khavanin, A, Variani, Improving the thermal and hydrophobic properties of bamboo biocomposite as sustainable acoustic absorbers, *Scientific Reports*, 2025, **15**, 3148, doi: 10.21203/rs.3.rs-5110931/v1.
[29] F. Huang, B. Motealleh, D. Wang, C. Cornelius, Tailoring intrinsic hydrophobicity and surface energy on rough surface via low-T Cassie-Wenzel wetting transition method, *AIChE Journal*, 2023, **69**, e17908, doi: 10.1002/aic.17908.
[30] Y. Chen, X. Ye, D. Wang, J. Yang, C. Wu, J. Xu, H. Yang, Z. Shi, Stepwise modification with 2,3-epoxypropyltrimethylammonium chloride cationization and rosin acid impregnation to improve water repellency and mold-proof property of bamboo, *Industrial Crops & Products*, 2023, **193**, 116248, doi: 10.1016/j.indcrop.2023.116248.
[31] Q. Yang, W. Su, J. Hu, Y. Xu, Z. Liu, L. Hui, Synthesis of Superhydrophobic Cellulose Stearoyl Ester for Oil/Water Separation, *Nanomaterials*, 2022, **12**, 1964, doi: 10.3390/nano12121964.
[32] H. Xu, F. Qiu, W. Han, Z. Xue, Study on the effect of lignin removal rate on the dielectric properties of delignified materials, *Coatings*, 2024, **14**, 1421, doi: 10.3390/coatings14111421.
[33] H. Zhao, J. Tang, Z. Li, T. Xiong, T. Zhou, Advancing bamboo fiber reinforcement: A novel approach using eco-friendly plant ash alkali treatment, *International Journal of Biological Macromolecules*, 2024, **283**, 137590, doi: 10.1016/j.ijbiomac.2024.137590.
[34] Q. Lin, Y. Huang, W. Yu, Effects of extraction methods on morphology, structure and properties of bamboo cellulose, *Industrial Crops and Products*, 2021, **169**, 113640, doi: 10.1016/j.indcrop.2021.113640.
[35] Q. Lin, P. Jiang, S. Ren, S. Liu, Y. Ji, Y. Huang, W. Yu, G. Fontaine, S. Bourbigot, Advanced functional materials based on bamboo cellulose fibers with different crystal structures, *Composites Part A: Applied Science and Manufacturing*, 2022, **154**, 106758, doi: 10.1016/j.compositesa.2021.106758.
[36] I. Janker-Obermeier, V. Sieber, M. Faulstich, D. Schieder, Solubilization of hemicellulose and lignin from wheat straw through microwave-assisted alkali treatment, *Industrial Crops and Products*, 2012, **39**, 198-203, doi: 10.1016/j.indcrop.2012.02.022.
[37] M. Smith, L. Scudiero, J. Espinal, J.-S. McEwen, M. Garcia-Perez, Improving the deconvolution and interpretation of XPS spectra from chars by ab initio calculations, *Carbon*, 2016, **110**, 155-171, doi: 10.1016/j.carbon.2016.09.012.
[38] Y. Wu, B. Yuan, M. Li, W. Zhang, Y. Liu, C. Li, Well-defined BiOCl colloidal ultrathin nanosheets: synthesis, characterization, and application in photocatalytic aerobic oxidation of secondary amines, *Chemical Science*, 2015, **6**, 1873-1878, doi: 10.1039/c4sc03229b.
[39] J. U. Kiran, J. P. Roners, S. Mathew, XPS and thermal studies of silver doped SiO_2 matrices for plasmonic applications, *Materials Today: Proceedings*, 2020, **33**, 1263-1267, doi: 10.1016/j.matpr.2020.03.500.
[40] L. Zhang, J. Qiu, J. Deng, S. Song, Z. Hong, W. Jia, S. Huang,

X. Zeng, Efficient transformation of hemicellulosic biomass into sugar alcohols with non-precious and stable bimetallic support catalyst, *Industrial Crops and Products*, 2023, **194**, 116378, doi: 10.1016/j.indcrop.2023.116378.

[41] C. Shi, L. Zhang, Z. Shi, Z. Wang, J. Ma, Mechanistic investigation of cellulose regulating the morphology and photocatalytic activity of Al-doped ZnO, *International Journal of Biological Macromolecules*, 2023, **228**, 435-444, doi: 10.1016/j.ijbiomac.2022.12.222.

[42] N. Bian, X. Yang, X. Zhang, F. Zhang, Q. Hou, J. Pei, A complex of oxidised chitosan and silver ions grafted to cotton fibres with bacteriostatic properties, *Carbohydrate Polymers*, 2021, **262**, 117714, doi: 10.1016/j.carbpol.2021.117714.

[43] D. Puckhaber, J. H. Finke, S. David, B. Gururajan, S. Rane, A. Kwade, Effect of particle size on the dispersion behavior of magnesium stearate blended with microcrystalline cellulose, *International Journal of Pharmaceutics*, 2024, **651**, 123792, doi: 10.1016/j.ijpharm.2024.123792.

[44] J. Dun, H. Chen, C. Sun, Profound tabletability deterioration of microcrystalline cellulose by magnesium stearate, *International Journal of Pharmaceutics*, 2020, **590**, 119927, doi: 10.1016/j.ijpharm.2020.119927.

[45] K. Yang, X. Zhang, D. Zu, H. Zhou, J. Ma, Z. Yang, Shifting Emphasis from Electro-to Catalytically Active Sites: Effects of Pore Size of Flow-Through Anodes on Water Purification, *Environmental Science & Technology*, 2023, **57**, 20421-20430, doi: 10.1021/acs.est.3c07448.

[46] X. Wei, J. Yuan, G. Wang, F. Chen, X. Chen, H. Jiang, L. M. Smith, J. Deng, Effect of chemical composition and cell structure on water vapor sorption behavior of parenchyma cells and fiber cells in moso bamboo (Phyllostachys edulis), *Industrial Crops and Products*, 2022, **178**, 114652, doi: 10.1016/j.indcrop.2022.114652.

[47] J. Dun, F. Osei-Yeboah, P. Boulas, Y. Lin, C. C. Sun, A systematic evaluation of poloxamers as tablet lubricants, *International Journal of Pharmaceutics*, 2020, **576**, 118994, doi: 10.1016/j.ijpharm.2019.118994.

[48] R. Kumar, J. S. Chohan, R. Kumar, A. Yadav, Piyush and P. Kumar, Metal spray layered hybrid additive manufacturing of PLA composite structures: Mechanical, thermal and morphological properties, *Journal of Thermoplastic Composite Materials*, 2020, **35**, 1387-1407, doi: 10.1177/0892705720932622.

[49] S. Wang, X. Guo, X. Zhang, H. Lu, H. Liu, Experimental study on biomass reactive drying based on three major components: Cellulose, hemicellulose, and lignin, *Chemical Engineering Journal*, 2025, **504**, 158675, doi: 10.1016/j.cej.2024.158675.

[50] X. Ye, Y. Chen, J. Yang, H. Yang, D. Wang, B. B. Xu, J. Ren, D. Sridhar, Z. Guo, Z. Shi, Sustainable wearable infrared shielding bamboo fiber fabrics loaded with antimony doped tin oxide/silver binary nanoparticles, *Advanced Composites and Hybrid Materials*, 2023, **6**, 106, doi: 10.1007/s42114-023-00683-8.

[51] L. Badra, I. Epstein, Propagation behavior of silver hydroxide precipitate band, *Chemical Physics Letters*, 2022, **800**, 139681, doi: 10.1016/j.cplett.2022.139681.

[52] F. Foadi, N. Celik, A. Esidir, M. S. Onses, Roughness-dependent hydrophobicity of polydimethylsiloxane grafted titanium thin films, *Surface and Coatings Technology*, 2024, **483**, 130749, doi: 10.1016/j.surfcoat.2024.130749.

[53] L. Zhang, Z. Chen, First principles investigation on long alkyl chain-based surface anchoring for self-assembled bilayer, *Applied Surface Science*, 2020, **506**, 144692, doi: 10.1016/j.apsusc.2019.144692.

[54] C. Yao, S. Tang, D. Sebastian, R. Tadmor, Sliding of water droplets on micropillar-structured superhydrophobic surfaces, *Applied Surface Science*, 2020, **504**, 144493, doi: 10.1016/j.apsusc.2019.144493.

[55] M. Dasaev, O. Kalakutskaya, O. Zilova, A. mednikov, effect of ultrasonic cleaning after laser texturizing of surface of AISI 316L steel on the degree of wetting and corrosion resistance, *Coatings*, 2023, **13**, 2058, doi: 10.3390/coatings13122058.

[56] J. Wu, Z. Yixiu, T. Zhong, W. Zhang, H. Chen, Bamboo slivers with high strength and toughness prepared by alkali treatment at a proper temperature, *Journal of Wood Science*, 2023, **69**, 13, doi: 10.1186/s10086-023-02084-3.

[57] R. A. Trbojevich, S. Khare, J. H. Lim, F. Watanabe, K. Gokulan, K. Krohmaly, K. Williams, Assessment of silver release and biocidal capacity from silver nanocomposite food packaging materials, *Food and Chemical Toxicology*, 2020, **145**, 111728, doi: 10.1016/j.fct.2020.111728.

[58] L. Li, Z. Bi, Y. Hu, L. Sun, Y. Song, S. Chen, F. Mo, J. Yang, Y. Wei, X. Wei, Silver nanoparticles and silver ions cause inflammatory response through induction of cell necrosis and the release of mitochondria in vivo and in vitro, *Cell Biology and Toxicology*, 2020, **37**, 177-191, doi: 10.1007/s10565-020-09526-4.

[59] A. Li, G. Wang, Y. Zhang, J. Zhang, W. He, S. Ren, Z. Xu, J. Wang, Y. Ma, Preparation methods and research progress of superhydrophobic paper, *Coordination Chemistry Reviews*, 2021, **449**, 214207, doi: 10.1016/j.ccr.2021.214207.

Open Access